Materials Letters 230 (2018) 195–198

Contents lists available at ScienceDirect

Materials Letters

journal homepage: www.elsevier.com/locate/mlblue

Time-resolved fractal dimension analysis in ferroelectric copolymer thin films using R-based image processing

Seonhyoung Kim [a,1], Kwang-Won Park [a,1], Ho-young Woo [b], Jongin Hong [a,*]

[a] Department of Chemistry, Chung-Ang University, 84 Heukseok-ro, Dongjak-gu, Seoul 06974, Republic of Korea
[b] Department of Applied Statistics, Chung-Ang University, 84 Heukseok-ro, Dongjak-gu, Seoul 06974, Republic of Korea

ARTICLE INFO

Article history:
Received 9 May 2018
Received in revised form 27 July 2018
Accepted 28 July 2018
Available online 30 July 2018

Keywords:
Ferroelectric
P(VDF-TrFE)
PFM
Fractal dimension

ABSTRACT

We have developed time-resolved fractal dimension analysis in ferroelectric copolymer films in order to understand the effect of polarization relaxation on domain wall roughness. Interestingly, the progressive polarization relaxation of irregular domains results from the domain back reversal at the boundaries where the antiparallel polarization encounters, and therefore has a significant influence on the fractal dimension of the irregular domains as a function of time.

1. Introduction

Ferroelectric polymers have attracted significant interest for emerging applications, such as flexible memories, energy harvesters and electronic skins [1–6]. Among the numerous ferroelectric polymers, poly(vinylidene fluoride) (PVDF) and its copolymers with trifluoroethylene (TrFE) are very notable not only for their relatively large remnant polarization values but also for their transparency and flexibility [7,8]. Recently, nanoscale phenomena in the P(VDF-TrFE) thin films have been explored by piezoresponse force microscopy (PFM) which probes bias-induced surface displacement and visualizes ferroelectric domain structures [9–12]. PFM allows us to understand polarization reversal mechanisms and domain wall dynamics at nanoscale. The progressive polarization loss in the ferroelectric polymer films has been studied in terms of switching dynamics or stability of written polarization states. However, its effect on domain shape and domain wall roughness has not been fully investigated.

Previously, we demonstrated that the fractal dimension analysis of irregular domains was very valuable for understanding the evolution of the domain geometry in the switching process [11]. An important issue in the aforementioned applications would be time-dependent change in ferroelectric properties. In this study, we report time-resolved fractal dimension analysis in the P(VDF-TrFE) thin films to understand the effect of polarization relaxation on domain wall roughness. We also suggest a new image processing algorithm based on the EBImage package in R to extract domain structural parameters, such as domain size and perimeter, for fractal dimension analysis and verify its efficacy on the time-dependent fractal dimension analysis with massive data.

2. Experimental

The detailed preparation of P(VDF-TrFE) films is described elsewhere [12]. Its microstructure was investigated by transmission electron microscopy (TEM), Fourier transform infrared (FTIR) spectroscopy and X-ray diffraction (XRD). PFM measurements were performed using a commercial atomic force microscope (AFM, XE-120, Park Systems) equipped with a lock-in amplifier (SR830, Stanford Research System). An ac modulation voltage of 1 V_{rms} at 17 kHz was applied to a Pt/Ir-coated Si tip (PPP-CONTPt, Nanosensors, force constant $k \approx 0.2\ N\ m^{-1}$). A scan area of 5 μm × 5 μm was switched as upwards at −7 V to the AFM tip and then a series of pulses with different positive voltage and pulse widths were applied to the tip in the background poling area to form downward dot domains. Subsequently, PFM amplitude and phase images were simultaneously taken by scanning 4.0 μm × 4.0 μm with 512 × 512 pixels as a function of time. The relative humidity (RH) in the chamber was kept 40% during the PFM measurements. In the PFM amplitude images, the bright regions indicate domains with strong out-of-plane polarization orienting either downward or upward. The dark regions are mainly observed near the domain

* Corresponding author.
E-mail address: hongj@cau.ac.kr (J. Hong).
[1] Equal contribution to this article.

https://doi.org/10.1016/j.matlet.2018.07.125
0167-577X/

boundaries, where two opposite domains contribute equally to the tip vibration signal [12,13]. In the PFM phase images, the bright regions correspond to domains with upward polarization, whilst the dark regions represent domains with downward polarization. To determine fractal dimension of each domain, image processing was performed by using an EBImage package in R (R 3.3.1, GNU General Public License). R is a language and environment for statistical computing and graphics. The EBImage package is a toolbox of image processing and analysis for R. It features multi-dimensional image processing, a range of fast image processing, seamless integration with R's native array data structures and coherence of the user interface.

3. Results and discussion

In Fig. 1, the ferroelectric P(VDF-TrFE) film was uniformly fabricated on the platinized substrate and its thickness was 25 nm. In FTIR spectrum, ferroelectric polar β-phase was confirmed by the characteristic bands corresponding to *trans* sequences longer than TTTT (1290 cm^{-1}) and longer than TTT (1200 cm^{-1} and 889 cm^{-1}). In XRD, the prominent peak at $2\theta = 19.8°$ due to (1 1 0) and (2 0 0) reflections of the crystalline β-phase also was observed. Fig. 2 shows a schematic diagram of time-resolved fractal dimension analysis using our R-based algorithm. To obtain accurate area and perimeter of each written domain, a PFM phase image (i.e. a binary digital image) is converted into a three-column data containing horizontal position (X), vertical position (Y) and polarization direction (Z) of each pixel. It should be noted that a positive value indicates upward polarization and vice versa. Firstly, positive values in the Z column are assigned to 0 and negative ones are left unchanged. This is a 'domain isolation' step in our image processing, which separates a certain domain structure from the background and eliminate nuisance noise. Secondly, a new PFM phase image can be generated from the processed data and then the image is divided into 9 image tiles containing only single downward domain of interest. Thirdly, pixels of value 0 are considered as background (black) and other pixels are recognized as an object (grey) in the image tile for further analysis. The number of pixels corresponding to the object are obtained to calculate its perimeter (i.e. a path that surrounds a two-dimensional shape) and area. In this case, pixel length and area are 12.2 nm and 61 nm^2,

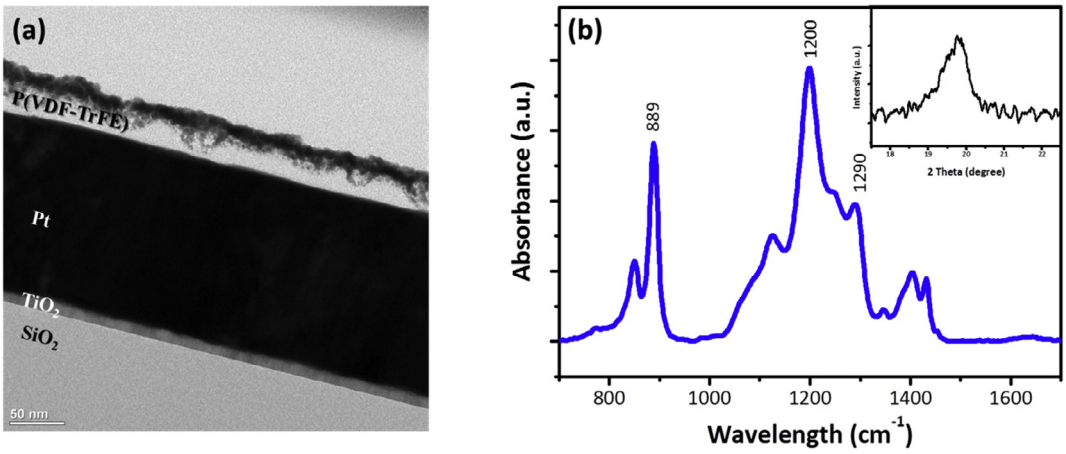

Fig. 1. (a) TEM cross-sectional image and (b) FTIR spectrum of the P(VDF-TrFE) film. The inset shows XRD patterns to determine its crystallinity.

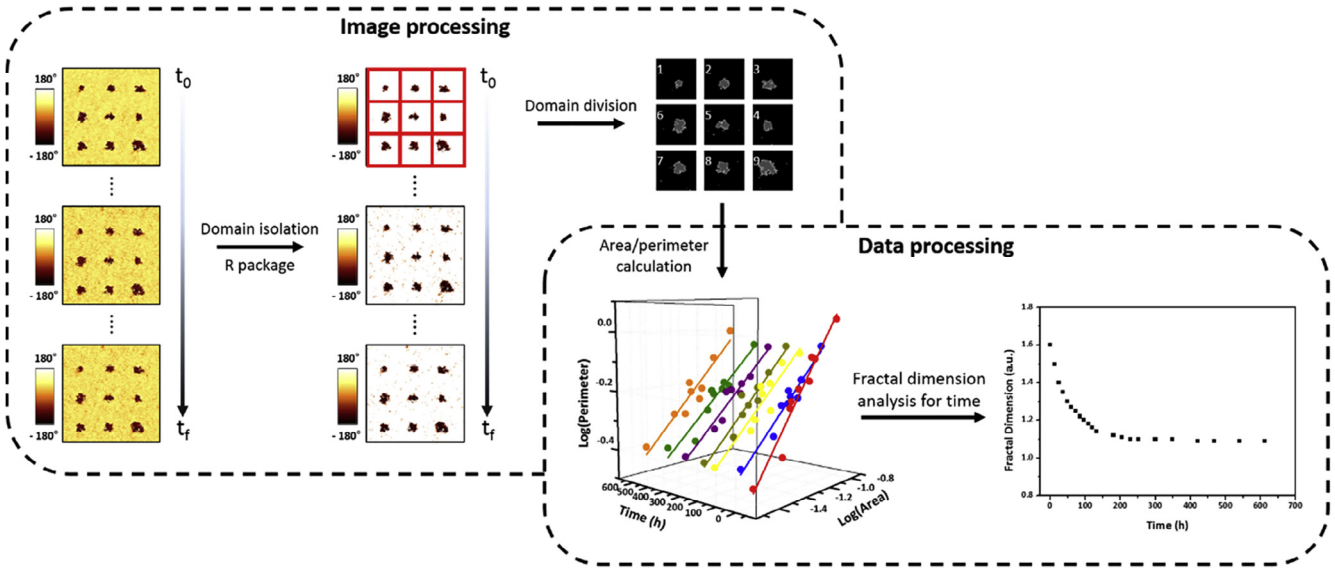

Fig. 2. A schematic diagram of time-resolved fractal analysis using PFM phase images.

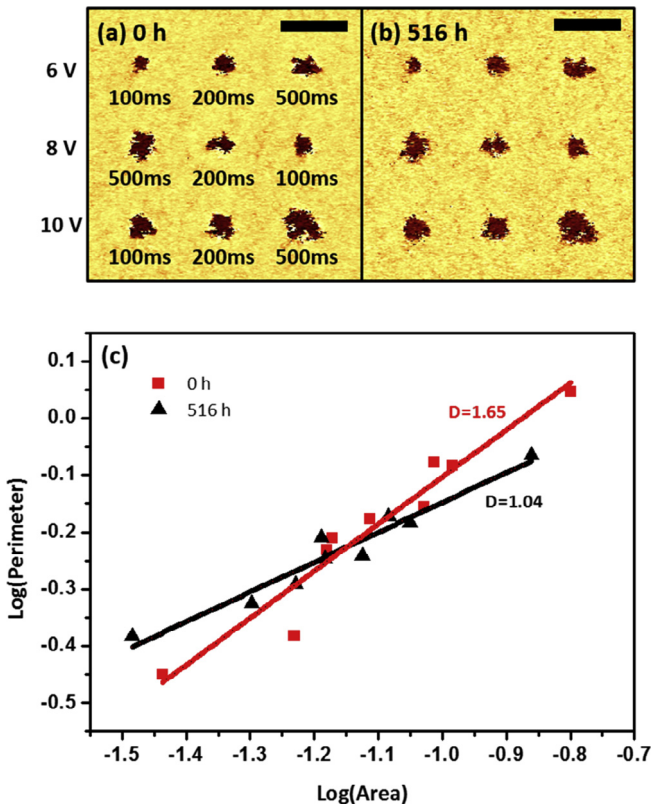

Fig. 3. PFM phase images of the downward domains formed at different conditions: pulse amplitude (6 V–10 V) and pulse width (100 ms to 500 ms): (a) 0 h and (b) 516 h. Scale bar is 1 μm. (c) Log-log plot of perimeter versus area at 0 h (red, square) and 516 h (black, triangle).

respectively. After obtaining all perimeters and area values of 9 single domains, the fractal dimension can be derived from the log-log plot of domain perimeter (P) versus area (A): $P = K \cdot A^{D/2}$ where K is a prefactor and D is dimensionality [12,14,15]. The fractal dimension yields numerical estimation of inhomogeneity and nonregularity of the object of interest. The series of steps are repeated to collect all fractal dimension values over time. Finally, we can conduct time-dependent fractal dimension analysis. Unfortunately, a commercial image processing software is somewhat inaccurate to extract perimeter and area values of a domain contaminated by nuisance noise (see Fig. S1).

Fig. 3 show PFM phase images of downward domains poled at different conditions. We examined switching behavior under poling conditions only for fully penetrated domains. Penetrated domains along the thickness direction could be generated by applying a least 6 V with 100 ms of pulse width. As the pulse voltage and width increased, the domain size and irregularity increased. The irregular domain wall would result from the adsorbed water on the junction area between the tip and the sample surface and its effect on lateral spread of the electric field [12,16,17]. The fractal dimension could be calculated from the slope of the log-log plot of domain perimeter versus area (Fig. 3c). The slope indicates the degree of disorder for the downward domain. If the domain structure is perfectly circular, its fractal dimension value is approximately one ($D = 1$). If the domain structure becomes irregular, the value is close to two ($D = 2$). When comparing two PFM phase images of virgin and 516 h, the fractal dimensions were 1.65 and 1.22, respectively.

Fig. 4a illustrates the evolution of the downward domain with the lapsed time. Interestingly, the irregular virgin domain gradually became smooth. We think that this change results from domain reversal. The lateral movement of the domain boundary could be monitored in the PFM amplitude images over time. Reversed domains preferentially nucleated at the domain boundaries, where the antiparallel polarization encounters, and the head-to-head polarization structure could induce depolarization field. When the curvature of the domain wall is large, the domain wall moves to minimize its energy [18]. Accordingly, the progressive polarization relaxation would have an influence on the perimeter and area of the written domain and therefore its fractal dimension. Fig. 4b shows fractal dimension as a function of time. The fractal dimension rapidly decreased in early time and then slowly decayed. We employed a stretched exponential model to investigate such fractal dimension relaxation phenomena.

$$D(t) = \mathrm{A} \cdot \exp\left(-\left(\frac{t}{\tau}\right)^{n}\right) + D_0 \quad (1)$$

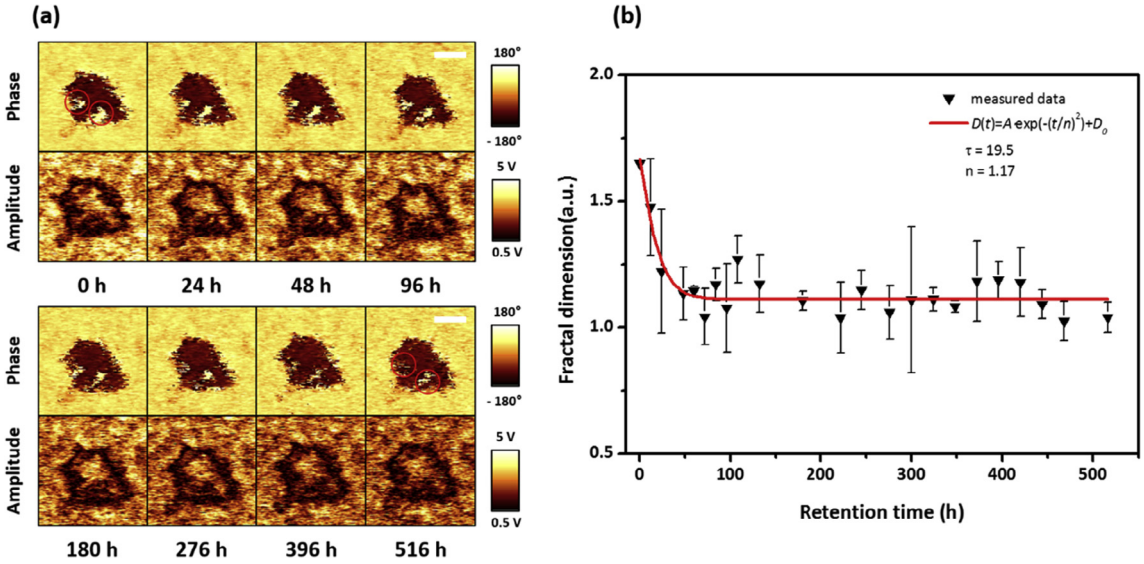

Fig. 4. (a) PFM phase and amplitude images of the downward down formed with 10 V of pulse amplitude and 500 ms of pulse width as a function of time. Scale bar is 300 nm. (b) Time-dependent change in fractal dimension of the downward domain.

where $D(t)$ is the dimensionality of domains correlated to time, A is the amplitude of the exponential function, τ is the relaxation time, n is the characteristic exponent and D_0 is saturated fractal dimension of retained domains. The fitting result obtained using Eq. (1) is denoted as a solid line in Fig. 4b. The exponent behavior with $n > 1$ is dominated by the domain back reversal to redistribute the charges and suppress the electric field built in the ferroelectric layer [19], which is distinct from a dispersive transport or random walk-type process with $0 < n < 1$.

4. Conclusions

In summary, we demonstrated time-resolved fractal dimension analysis to understand the effect of polarization relaxation on domain wall roughness. We also verified the efficacy of our new image processing algorithm based on the EBImage package in R to quickly determine the change in fractal dimension of the irregular domains as a function of time. We will further explore the effect of humidity on the time-dependent change of fractal dimension in the ferroelectric films.

Acknowledgements

This research was supported by the National Research Foundation of Korea funded by the Ministry of Science and ICT (No. 2014M3A9B8023478, No. 2017M2A8A1066682, No. 2017M2B2A4049901) and the Chung-Ang University Graduate Research Scholarship (2017).

Appendix A. Supplementary data

Supplementary data associated with this article can be found, in the online version, at https://doi.org/10.1016/j.matlet.2018.07.125.

References

[1] Y.J. Park, I. Bae, S.J. Kang, J. Chang, C. Park, IEEE Trans. Dielectr. Electr. Insul. 17 (2010) 1135–1163.
[2] S.-T. Han, Y. Zhou, V.A.L. Roy, Adv. Mater. 25 (2013) 5425–5449.
[3] D. Kim, S. Hong, D. Li, H.S. Roh, G. Ahn, J. Kim, M. Park, J. Hong, T.H. Sung, K. No, RSC Adv. 3 (2013) 3194–3198.
[4] S.K. Ghosh, A. Biswas, S. Sen, C. Das, K. Henkel, D. Schmeisser, D. Mandal, Nano Energy 30 (2016) 621–629.
[5] X. Han, X. Chen, X. Tang, Y.-L. Chen, J.-H. Liu, Q.-D. Shen, Adv. Funct. Mater. 26 (2016) 3640–3648.
[6] L. Seminara, L. Pinna, A. Ibrahim, L. Noli, S. Caviglia, P. Gastaldo, M. Valle, Mechatronics 34 (2016) 84–94.
[7] V.V. Kochervinskii, Crystallogr. Rep. 48 (2003) 649–675.
[8] M. Poulsen, S. Ducharme, I.E.E.E. Trans, Dielectr. Electr. Insul. 17 (2010) 1028–1035.
[9] J.R. Brian, S. Jesse, S.V. Kalinin, J. Kim, S. Ducharme, V.M. Fridkin, Appl. Phys. Lett. 90 (2007) 122904.
[10] Y. Kim, W. Kim, H. Choi, S. Hong, H. Ko, H. Lee, K. No, Appl. Phys. Lett. 96 (2010) 012908.
[11] Y.Y. Choi, J. Hong, D.-S. Leem, M. Park, H.W. Song, T.-H. Sung, K. No, J. Mater. Chem. 21 (2011) 5057–5061.
[12] K.-W. Park, H. Seo, J. Kim, D. Seol, J. Hong, Y. Kim, Nanotechnology 25 (2014) 355703.
[13] J. Kim, K.-W. Park, J. Hong, K. No, Appl. Surf. Sci. 334 (2015) 165–168.
[14] B.J. Rodriguez, S. Jesse, A.P. Baddorf, S.-H. Kim, S.V. Kalinin, Phys. Rev. Lett. 98 (2007) 247603.
[15] M.K. Roy, J. Paul, S. Dattagupta, J. Appl. Phys. 108 (2010) 014108.
[16] C. Blaser, P. Paruch, New J. Phys. 17 (2015) 013002.
[17] A.V. Ievlev, A.N. Morozovska, V.Ya. Shur, S.V. Kalinin, Appl. Phys. Lett. 104 (2014) 092908.
[18] A.J. Bray, Adv. Phys. 43 (1994) 357–459.
[19] A. Morelli, S. Venkatesan, G. Palasantzas, B.J. Kooi, J.Th.M. De Hosson, J. Appl. Phys. 102 (2007) 084103.